Probability density functions, skewness, and flatness in large Reynolds number turbulence

P. Tabeling, G. Zocchi, F. Belin, J. Maurer, and H. Willaime
Laboratoire de Physique Statistique, Ecole Normale Superieure, Laboratoire associé au CNRS, à l'ENS, aux Universités Paris 6 et Paris 7, 24 rue Lhomond, 75005 Paris, France
(Received 31 October 1994; revised manuscript received 16 August 1995)

Probability density functions (PDF) of longitudinal velocity increments are measured in an experiment using low temperature helium gas, in which a large domain of microscale Reynolds numbers R_λ (from 150 to 5040) is explored. The technique of measurement, which is essentially hot wire anemometry, but operating in nonstandard conditions, is described. In the inertial range of scales, and for a given scale of separation, the PDF are found to be independent of the Reynolds number at large R_λ. Measurements of the skewness and the flatness of the velocity derivatives are performed in a range of R_λ lying between 150 and 3200. The surprising result that we find is that these quantities first increase with the Reynolds number up to $R_\lambda \approx 700$ and then cease to increase further, indicating a transitional behavior.

PACS number(s): 47.27.−i, 47.55.Bx, 47.80.+v

I. INTRODUCTION

In the field of turbulence, an important part of the research effort is devoted to small scale intermittency [1]. These last years, several numerical and experimental studies have brought about interesting information, and indeed one may hope that this will generate significant progress in the understanding of this striking phenomenon. On the experimental side, effort has been made to characterize the probability density functions of the longitudinal velocity increments (which are a rich diagnostics of intermittency) [2]. It is generally observed that, deep in the inertial domain, the tails of such distributions have the form of stretched exponentials [2]. More specifically, their form and their dependence with the scale have been recently discussed [3]. Concerning the skewness and flatness of the velocity derivatives, the results are more scarce. Most of our knowledge on these quantities relies on a compilation of laboratory and atmospheric data prepared, 15 years ago, by Van Atta and Antonia [4]. This compilation shows, as a clear trend, that the flatness of the velocity derivative increases with the Reynolds number at large Reynolds numbers. This trend also exists for the skewness, but is less pronounced. These results are often considered as forming a sort of cornerstone for the phenomenology of small scale intermittency. The compilation of Ref. [4] has been widely used to inspire and constrain models [5]. Concerning the spatial aspects associated with small scale intermittency, they have been illuminated by recent numerical [6] and physical [7] experiments: vortex filaments have been identified as forming an important part of the structures associated with intermittency, at least for moderate Reynolds numbers [6]. One can probably distinguish (but this is under discussion) two generations of filaments, the primary one, whose scale belongs to the inertial domain, and the works, which may result from the instability of the previous ones, and whose diameter is a few Kolmogorov scales [8]. The link between these objects and the statistical properties of the flow is currently under debate, and is an important issue in this domain of turbulence.

In the experiment we describe herein, it is possible, by working with low temperature helium, to investigate a range of microscale Reynolds numbers lying between 150 and 5040 (but restricted to 150–3200 for dissipative range quantities), with the same flow configuration. The objective of the present paper is to report the results obtained, in this setup, about the evolution of some diagnostics of small scale intermittency, such as the probability density functions (PDF's) of the longitudinal velocity increments, and the skewness and flatness of the velocity derivatives, with the Reynolds number.

II. EXPERIMENTAL SETUP

Since the two setups have been described elsewhere [9,10], here we give a brief presentation of them. The flow is schematically represented on Fig. 1: it is confined in a cylinder, which is limited axially by disks equipped with blades. The disks are driven by independent dc motors, and turbulence is produced by rotating the two disks in opposite directions. We shall name the smaller cell "cell 1" and the larger one "cell 2." In the smaller one, the working volume (where turbulence is prepared) is 6.6 cm in diameter and 5.5 cm in height, and in the larger one it is 20 cm in diameter and 13.1 cm high. The two cells thus have slightly different aspect ratio height over radius—0.76 and 0.60, respectively, for cells 1 and 2. There exist other differences between the two cells, such as the number of blades (eight for cell 1 and six for cell 2) and the presence or the absence of rims fixed to the rotating disks. Each cell is enclosed in a cylindrical vessel, in thermal contact with a liquid helium bath. The temperature of the experiment is regulated at a constant value, comprised between 4.2 and 8 K. The vessel is filled with helium gas, at a controlled pressure, ranging from 0 up to 6 atm. It is remarkable to mention that, in the present system, within the cells, the standard deviation of the temperature fluctuations is lower than 1 mK.

The measurements are performed by using hot wire

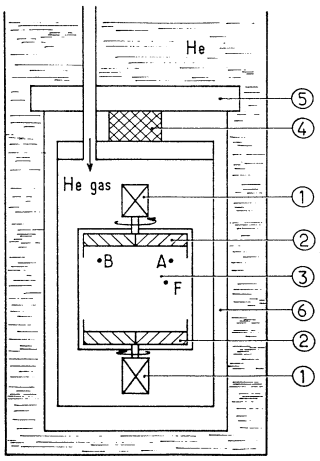

FIG. 1. Sketch of the experiment. (1) dc motors. (2) Blades fixed on the rotating disks. (3) Working fluid. (4) Thermal link. (5) Copper plate. (6) Vacuum.

anemometry (see below for a discussion of the technique). The velocity is measured at several points, in the two setups: the table below shows the probes we use, together with their position in the cell, in cylindrical coordinates (here R and H, respectively, are the radius and height, and $z=0$ is the symmetry plane). We also give the wire length for each probe.

probe name	l_w (μm)	r/R	θ	z/H
1	50	0.72	0	−0.3
2	7	0.72	π	0.3
A	27	0.65	0	0.34
B	7	0.65	π	0.34
F	15	0.5	0	0.18
A'	7	0.66	0	0.34

There are thus several sensors but the most important part of the measurements reported herein are performed by probes B and A'. In the series of experiments performed with sensor A', we have introduced a small mean rotation so as to displace the mixing layer respectively to the probe, thus offering the possibility to work with lower fluctuation rates. For this series, the corresponding turbulence level is typically 20%.

We have some strong indications on the large scale structure of the flow, although one cannot say, at the present time, that it is documented at a level comparable to more traditional configurations, such as jets or grid turbulence. Close to the disks, the flow is essentially a solid rotation and, in the central part, a mixing layer takes place. The large scale structure of the flow can be viewed as a confined circular mixing layer [10]; one actually must consider that this is a simplification of the flow structure, which is presumably acceptable only at a reasonable distance from the blades and from the walls. The integral scale (defined—somewhat arbitrarily— as the ratio between the limiting value of the velocity spectrum at small wave number and the square of the rms of the velocity fluctuation) is found to be independent of the Reynolds number: it is 4.5 cm in the large system and 1.5 cm in the smaller one. The fluctuation rate depends on the position, and varies from one experiment to the other, but we have not observed any systematic dependence with the Reynolds number. One finds, in the average, 35% for probe B [10] in the large cell, 20% for probe A', and 23% for sensors 1 and 2. The microscale Reynolds number R_λ and the Kolmogorov scale η are estimated locally by using the structure function of order 3 [10]. The following table gives values of some physical parameters of interest: for the large experiment (cell 2), we indicate the minimum and maximum values of R_λ and two typical values, and for the smaller one (cell 1), we report two typical values. In this table, ν is the kinematic viscosity, U is the mean velocity, u the fluctuation, Re is calculated by using the rotation rate and the radius as characteristic quantities, and λ is the Taylor microscale.

Cell	probe	ν (cm^2/s)	U (cm/s)	u (cm/s)	Re	R_λ	u/U	λ (μm)	η (μm)
2	B	0.105	84	22	13 700	174	0.26	8300	312
2	B	2.1×10^{-2}	284	94	2.3×10^{5}	674	0.33	1520	26
2	B	6.1×10^{-4}	102	34	2.9×10^{6}	2200	0.33	400	4.1
2	B	3.3×10^{-4}	136	52	7×10^{6}	5040	0.38	320	2
2	A'	5.5×10^{-4}	116	20	6×10^{6}	1382	0.17	360	4.9
2	A'	1.1×10^{-3}	64	13	2×10^{6}	822	0.21	680	12
1	2	2.7×10^{-2}	118	29	16 700	188	0.25	1740	64
1	2	2.6×10^{-4}	27.4	6.1	4.3×10^{5}	879	0.22	187	5

Since we work, in several cases, with unusually large fluctuation rates (particularly with probe B), it proved interesting to examine the velocity distributions in order to check whether the negative velocity fluctuations are correctly measured. Such histograms also are useful to detect the presence of large scale intermittency. Figure 2 shows one histogram, obtained for $R_\lambda=992$ using probe A'. One can see that the distribution is nearly Gaussian, and that the negative branch seems to be correctly resolved; this inspection allowed us to reject several

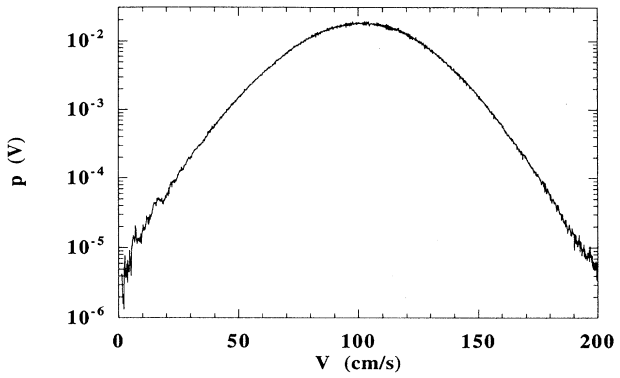

FIG. 2. A typical velocity distribution; here we use probe A'; $R_\lambda = 992$, and the fluctuation rate is 22%.

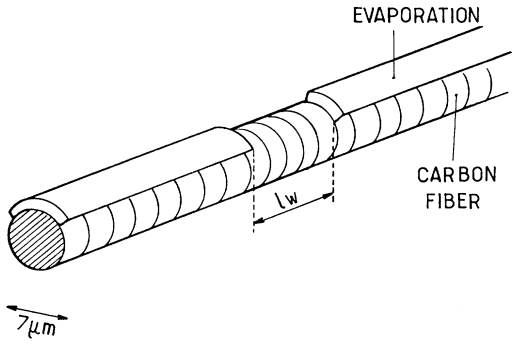

FIG. 3. Sketch of the active part of the sensor.

files—those for which the negative branch is partially absent, or the asymmetry is strong, or bumps exist on the tails.

III. "HOT" WIRE ANEMOMETER

Measuring local velocity in our system is delicate because we work at low temperature; the scales which would be desirable to resolve are of the order of several microns, and the frequencies of interest are quite high (several kHz). The technique which we use is essentially hot wire anemometry, operating in nonstandard conditions; here we discuss the differences between the standard situation and our case. To characterize the sensor, we also calculated the thermal field around the probe and the heat transfer, for stationary and nonstationary flows (this was done by using a commercial computer code FLUENT); we shall not report the detail of this study, just refer to it when necessary.

The anemometers are made from a carbon fiber, 7 μm in diameter, stretched across a rigid frame, of dimensions 5×5 mm. A double layer chromium-gold or silver-gold, evaporation, of typical thickness 1000 Å, covers the fiber everywhere except on a spot at the center, which thus defines the active length of the probes (see Fig. 3). Such lengths vary from 7 to 50 μm, from one sensor to the other. To check whether the geometrical length (which is imposed by the mask used during the evaporation process and checked with a microscope) is the effective length of the probe, we measure the resistance of the probe at various temperatures, as well its derivative with respect to temperature, at low temperatures. An acceptable probe is the one which shows consistency between these measurements. We further take the geometrical length to characterize the spatial resolution of the probe (denoted by l_w), but one must consider that this is only an approximation—probably accurate within 30% for the shortest probe—which does not incorporate end effects.

The electronics is home made, and is essentially a constant-temperature circuit; one must mention the presence of a capacitance, placed in parallel with a resistance of the bridge, which allows us to reduce the time response of the system. For the few files that have been obtained without capacitance, we introduce a correction on the data themselves when necessary. As for standard anemometers, we can impose the overheating. We have compared various overheatings, ranging from 3 to 15 K, and found it preferable to use rather large overheatings (lying between 5 and 15 K) for reasons which will be justified below. The overheating coefficient which we use is thus unusually large, since it ranges between 1 and 3 (while this parameter does not exceed 1 for standard anemometers). The signal is digitized on a 16 bit converter, controlled by a Digital Signal Processing card. The slope of the transfer function of the antialiasing filter, placed before the converter, is −125 dB/decade. The records are of various sizes, from a few ten millions to 10^{10} points.

The calibration of the probes are performed by driving the two disks in the corotating mode, at the same rotation rate, and assuming rigid rotation. We typically obtain calibration curves which can be very well fitted by using King's law formula (an example is given in [9]). One important difference with ordinary hot wire anemometry is that we operate at larger wire Reynolds numbers R_w, defined by

$$R_w = \frac{Ud}{\nu} ,$$

in which ν is the kinematic viscosity of the fluid, evaluated at the fluid temperature, far from the probe. Figure 4 shows the evolution of this parameter as a function of the microscale Reynolds number R_λ for cells 1 and 2. The typical values are much larger than for ordinary hot wires; vortex shedding presumably occurs at $R_\lambda = 800$ for the small setup and $R_\lambda = 1500$ for the large one. The influence of such a high Reynolds number on the measurement is not well documented even for standard anemometry. We have assumed that the conditions of measurement are acceptable since in our case, the Strouhal frequency does not interfere with the turbulent spectrum. We have found further support for this assumption by checking that the two cells give the same results despite the fact that the probes operate at different R_w.

The response time of the probe is a crucial issue; in ordinary hot wire anemometry, one defines the following

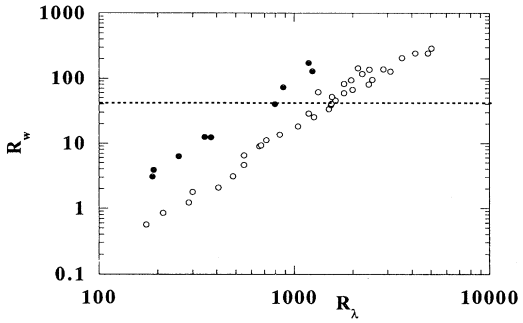

FIG. 4. Evolution of R_w with R_λ for the two cells: ○, cell 2; ●, cell 1; the dashed line represents the presumed onset of vortex shedding behind the probe.

time constants [11]: τ_1 (the time for the flow to pass the wire), τ_2 (the time for a velocity fluctuation to diffuse through the viscous boundary layer around the wire), τ_3 (the time for the thermal boundary layer around the wire to reach a new state after a velocity change), τ_4 (the time for heat to diffuse within the wire), and τ (the Kolmogorov time scale, defined by η/U). To fix the ideas, here we give estimates for such quantities, for a flow at 1 m/s, in the large cell, under 1 bar, at 5 K using a probe overheated at 20 K (the corresponding value of R_λ is roughly 1000):

$$\tau_1 \sim \tau_2 \sim \frac{d}{U} \sim 7\ \mu\text{s}\ , \quad \tau_3 \sim 1\ \mu\text{s}\ ,$$

$$\tau_4 \sim 12\ \mu\text{s}\ , \quad \tau \sim 12\ \mu\text{s}\ .$$

Here τ_3 is estimated from a full three dimensional numerical simulation, and τ_4 is determined experimentally (by heating internally the probe). There is some evidence that τ_3 increases as the overheating decreases, because the heat diffusivity of helium gas in the thermal boundary layer increases with the temperature. This reason, together with the optimization of the signal over noise ratio, led us to use overheat ratios ranging between 1 and 3. From the above estimates, one can see that the limiting factor is τ_4. The reason is that carbon, at low temperature is a poor heat conductor; therefore, unlike the standard wires, the internal heat diffusion time, within the fiber, cannot be neglected. Another consequence, which is more favorable, is that we can work with short probes since the conduction along the fiber is much smaller than for ordinary wires. To stress this point, we introduce the characteristic length l_c for heat diffusion along the wire, defined by

$$l_c = d\left[\frac{k_w}{k_f \mathrm{Nu}}\right]^{1/2} ,$$

where k_w and k_f, respectively, are the wire and fluid thermal conductivities, and Nu is the Nusselt number characterizing the heat transfer between the probe and the fluid (see Hinze [11] for a more sophisticated definition of such a length). As a rough statement, one can say that end effects can be neglected if the wire length is much longer than l_c. In such problems, it is usual to estimate the fluid properties at the mean temperature between the wire and the fluid, far from the wire. In our case, for a fiber working at 20 K, at $R_\lambda = 1000$, we have $k_w \approx 10^{-3}$ W/cm K, $k_f \approx 10^{-4}$ W/cm K, and Nu ≈ 10, so that l_c is found typically to be of the order of the fiber diameter. The same calculation done for ordinary wires would give l_c one hundred times the wire diameter. This shows that, in our situation, it is possible to use small aspect ratios sensors (which allows to improve their spatial resolution) while respecting the constraints usually accepted in hot wire anemometry.

Figure 5 shows measurements of the response time constant τ^* of probe A' using the so-called square wave test (see, for instance, Lomas [11]). The evolution of this time constant is represented as a function of the difference between the probe resistance at 4.2 K and the operating value, under conditions covering (quite comfortably) the range of velocities we explore. The correspondence between the probe resistance and the fiber temperature can be roughly figured out by considering that the latter vary between 8 and 20 K in this series of experiments. The interesting result is the low values of τ^*, and its independence from the flow conditions. For the operating conditions we consider, the range of accessible frequencies lies between 20 and 65 kHz. In practice, we select the overheating so as to obtain an appreciable ratio signal over noise together with an acceptable time constant τ^* (i.e., smaller than or equal to the Kolmogorov time τ).

Since our sensors differ in many aspects from standard probes, and it will take time to settle (at a level comparable to standard hot wire anemometry) many aspects of the technique we use, we have defined several procedures to detect possible errors. There are essentially two: the first one is to check that the results are independent of the overheating; the second one, which is possible with low temperature helium, is to check that the energy spectra, obtained in the same cell for the same Reynolds number and the same fluctuation rate, but with different fluid

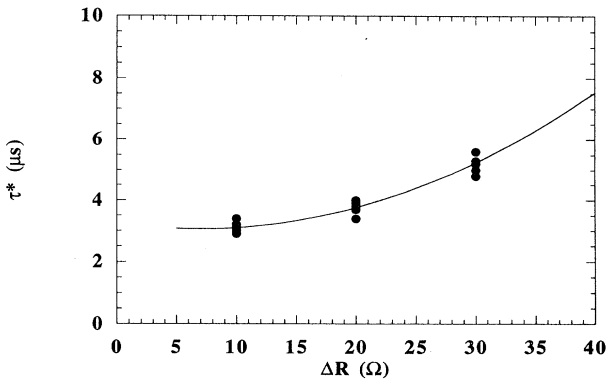

FIG. 5. Evolution of the time constant obtained by using the square wave test for probe A', for different flow conditions and overheatings. The resistance at 4.2 K is 320 Ω in this case. This test is performed with local velocity varying from 0 to 5 m/s, in the corotating mode, at 1 bar.

viscosities, collapse in the wave-number space. This allows us to detect whether there is a fixed time constant which affects the measurement. Figure 6 illustrates the second procedure: here we have two velocity spectra, plotted in the frequency domain, obtained for $R_\lambda = 530$ and a fluctuation rate of 20%. The frequency ranges which are covered are considerably different in the two cases. According to the overheating which we use, one can estimate that the frequency ranges which is accessible to the sensors is limited to 25 kHz. Plotting now in wave-number units (by using Taylor hypothesis), one can check that the two spectra collapse pretty well, up to a wave number corresponding to the maximum accessible frequency. The independency of the overheating, together with the satisfactory collapse of the spectra, make us confident about our measurements of dissipative range quantities in a domain of Reynolds number ranging between 150 and 1500. Beyond this range and up to 3200, we have not performed the second test, but the conditions of measurements are acceptable for dissipative range quantities. For inertial range quantities, since the working frequencies are lower, we shall present our results up to the largest value which we have achieved, i.e., 5040.

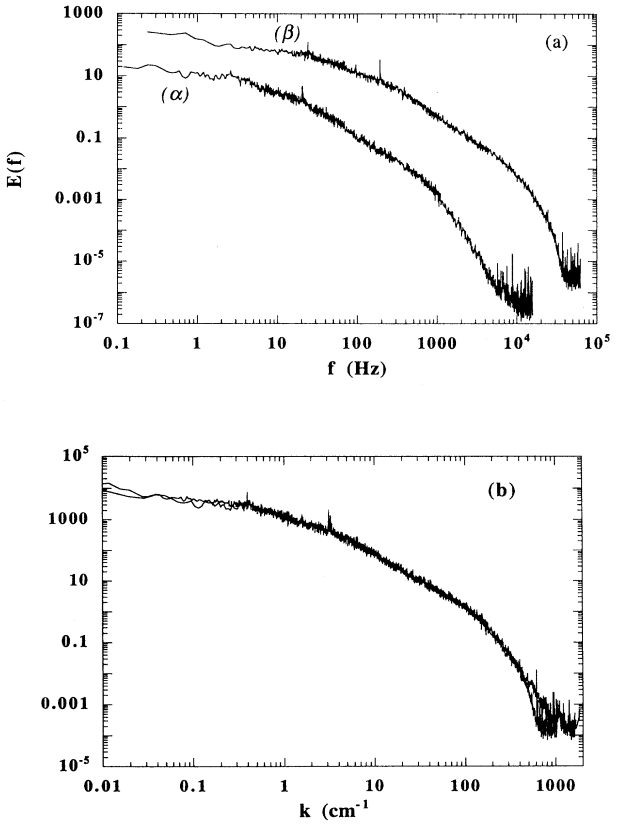

FIG. 6. Collapse of the spectra corresponding to the same Reynolds number $R_\lambda = 530$, but to two different viscosities (and thus to different mean velocities U_m). (a) (α) $U_m = 39$ cm/s; (β) $U_m = 383$ cm/s. (b) Collapse of the spectra plotted in the wave-number space (we have used an adjustment factor for the amplitudes).

IV. PROBABILITY DISTRIBUTION FUNCTIONS OF THE VELOCITY INCREMENTS

Figure 7 represents the probability density function (PDF) of the longitudinal velocity increments $\Delta V_r = V(x+r) - V(x)$ (where V is the local velocity) obtained for $R_\lambda \approx 3000$, for several separation lengths r, using sensor B. Here, we use the Taylor hypothesis to convert separation time τ into distances r (the precise form is $r = -U\tau$, where U is the mean local velocity). On such plots, we have

$$s = \frac{\Delta V_r}{\langle \Delta V_r^2 \rangle^{1/2}} ,$$

the brackets representing time averaging. s is thus a rescaled variable which ensures that the standard deviation of each PDF is equal to 1. As already noted in previous studies, the distributions evolve from a Gaussian shape to stretched exponentials as r decreases, evidencing the departure toward more intermittent profiles at smaller scales in the inertial range. The evolution of such a PDF with the Reynolds number is not straightforward to describe. The general form of the PDF reads

$$p = p\left[s, \frac{r}{R}, R_\lambda\right] , \tag{1}$$

where R is the cylinder radius. Distribution p fully depends on r/R, and R_λ in the general case. However, it appears that, for sufficiently large values of R_λ (i.e., for $R_\lambda > 1200$), the PDF seem to reach an asymptotic shape, independent of this parameter. This is shown in Fig. 8, which represents four PDF's, calculated for $r = 490$ μm, for four values of R_λ, comprised between 1200 and 4700; one obtains a collapse of the four curves on a single one. Although we have not performed a detailed study, one can fairly say that Fig. 8 is representative of the evolution of the PDF for r ranging between 30 times the Kolmogorov scale and 10 cm, which covers, in most cases, a domain extending from the lower edge (in terms of scale) of the inertial range to the integral scale. In the intermediate dissipative range, we observe a spread between

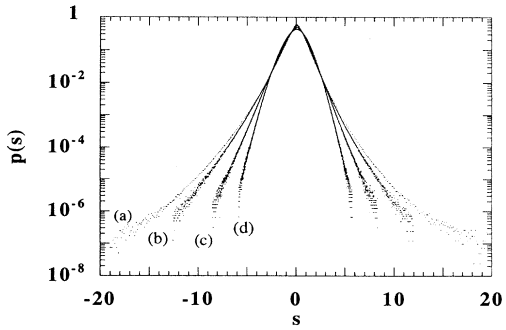

FIG. 7. Log linear plot of the PDF of the longitudinal increments of velocity, calculated on different scales (a) $r \approx 10$ μm. (b) $r \approx 100$ μm. (c) $r \approx 1$ mm. (d) $r \approx 1$ cm. The flow parameters are $\eta \approx 2.5$ μm and $R_\lambda \approx 3000$.

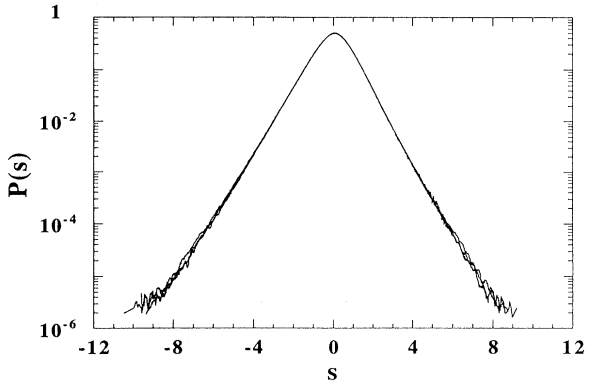

FIG. 8. Log linear plot of the PDF of the longitudinal increments of velocity, calculated for the same scales $r=490$ μm, and four values of R_λ: $R_\lambda=1260$, 2300, 2700, and 3700.

the PDF at different R_λ, which presumably reflects that the above property ceases to hold in this domain.

To describe the asymptotic shapes, we divide, somewhat arbitrarily, the PDF into two parts: one corresponding to the tails ($|s|>2$), and the other to the low increment region ($|s|<2$). The tip appears as parabolic, with a radius of curvature decreasing as the scale is decreased. Concerning the flanks, we find—in agreement with a previous study [3]—that they can be very well fitted by stretched exponentials of the form

$$p = A \exp(-\beta s^{\alpha}) , \tag{2}$$

in which A, α, and β are parameters, which depend on r

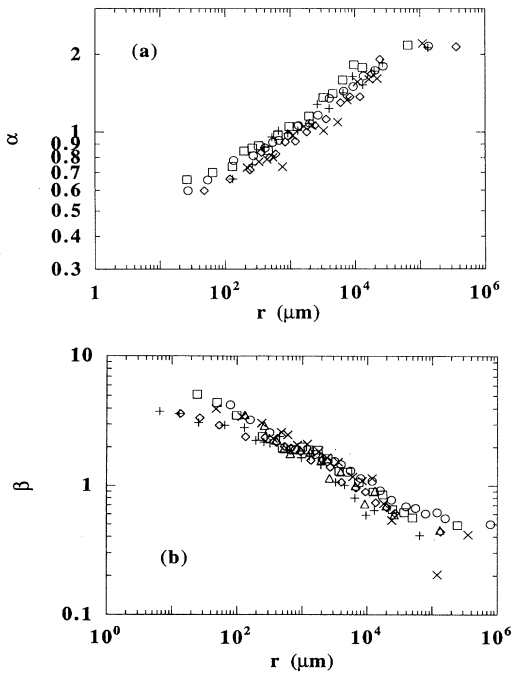

FIG. 9. Evolution of the parameters α [Fig. 3(a)] and β [Fig. 3(b)] with the scale r, for different values of R_λ. □, 1960; X, 4700; O, 1260; +, 3700; diamonds, 2100.

only. The quality of the fit is excellent for any value of r. The corresponding evolutions of α and β, for different values of R_λ, ranging from 1200 to 5000, is shown in Fig. 9, for the positive tail. There is some scatter in the data, but one can fairly say that, in the inertial range, the two parameters follow a single line, independent of R_λ. Much larger scatter is obtained when we use r/η instead of r as the variable. We thus may infer, on dimensional grounds, that the pertinent length is the integral scale in this range. Figure 9 shows that the exponent α increases with r/Λ, up to a limiting value of 2 (see Fig. 9); this value, which corresponds to the Gaussian limit, expresses the fact that as r increases, the two measurements of the velocity involved in the increment are statistically independent. The form of the curve of Fig. 9 as well as the limiting values, are in agreement with a recent analysis of atmospheric boundary layer data, carried out for a particular value of R_λ [3]. What we show here is that the corresponding curve is independent of the Reynolds number at large R_λ.

V. SKEWNESS AND FLATNESS OF THE VELOCITY DERIVATIVES

As previously mentioned, here we report only measurements performed in the range 150–3200, where the conditions of measurements of dissipative range quantities can be considered as acceptable.

The first method used to determine the skewness and flatness factors S and F of the velocity derivatives consist of calculating the following quantities:

$$S(r)=\frac{\langle \Delta V_r^3 \rangle}{\langle \Delta V_r^2 \rangle^{3/2}} \quad \text{and} \quad F(r)=\frac{\langle \Delta V_r^4 \rangle}{\langle \Delta V_r^2 \rangle^2} \tag{3}$$

defining S and F as the limiting values of such functions when r become small (in units of the Kolmogoroff scale). This defines a first method, which we call direct. $F(r)$ is also defined by

$$F(r)=\int_0^\infty s^4 p(s,r)ds=\frac{\int_0^\infty \Delta V_r^4 p'(\Delta V_r,r)d\Delta V_r}{\left[\int_0^\infty \Delta V_r^2 p'(\Delta V_r,r)d\Delta V_r\right]^2} ,$$

where p is the PDF of the normalized velocity increments introduced above, and p' the PDF of the (nonrenormalized) velocity increments. The above formula is interesting to quote because it allows us to check the statistical convergence of the results. This can be done by plotting the integrand $\Delta V_r^4 p'(\Delta V_r,r)$, and examining whether the tails are well converged. Figures 10(a) and 10(b) show the evolution of such an integrand, for two values of $R_\lambda - R_\lambda \approx 550$ and $R_\lambda \approx 2850$—and for two values of r lying in the dissipative range. In both cases, one may consider that convergence is achieved. This statement holds for all the other cases which we present here; one may say that, owing to the excellent stability of the experimental conditions, and the rapid time scales of the phenomenon we study, there is not much difficulty, in our case, in recording large files so as to achieve convergence of the moments.

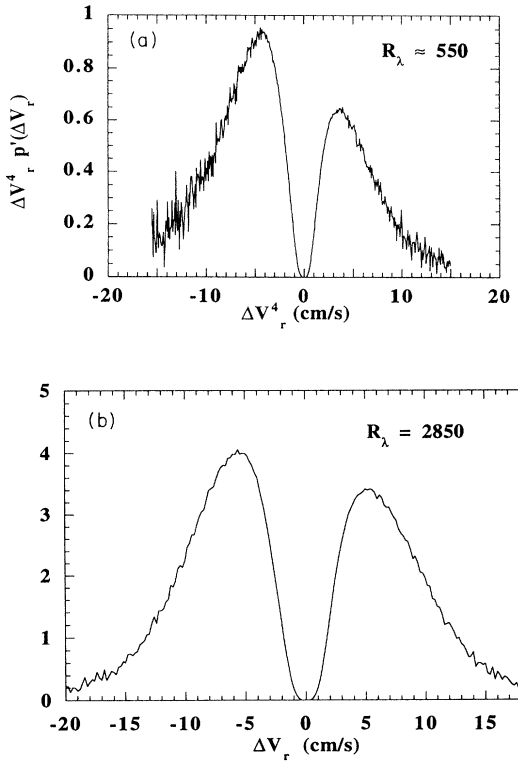

FIG. 10. Evolution of the integrand $\Delta V_r^4 p'(\Delta V_r, r)$ with ΔV_r for (a) $R_\lambda \approx 550$, $r/\eta = 1.7$ and (b) $R_\lambda \approx 2850$, $r/\eta = 3.8$.

Figure 11 represents the evolutions of $-S(r)$ and $F(r)$ for $R_\lambda \approx 1548$. We find that $-S(r)$ and $F(r)$ decrease with r as r/η increase; in both cases, the limiting values for large r/η is 3 for $F(r)$: this corresponds to the Gaussian limit which we expect for large separations. As r/η decreases toward 1, the functions $-S(r)$ and $F(r)$ tend to saturate; as previously mentioned, the corresponding limiting values define the skewness and flatness factors of the velocity derivatives.

It is interesting to consider another method of determination of S, which assumes that the Kolmogorov relation holds [12]; the corresponding expression for S reads [13]

$$S = -\frac{116\nu \int_0^\infty k^4 E(k)dk}{\left[15 \int_0^\infty k^2 E(k)dk\right]^{3/2}} = -116 \int_0^\infty (\eta k)^4 \Phi(\eta k) d(\eta k) , \quad (4)$$

where k is the wave number, $E(k)$ is the power density spectrum per unit of wave number, and Φ is the normalized spectrum function. According to relation (4), one must have

$$\tfrac{1}{15} = \int_0^\infty (\eta k)^2 \Phi(\eta k) d(\eta k) .$$

This defines a second method which we call spectral. Both methods (direct and spectral) are expected to give the same result when the range of scale involved in the integrand of (4) is isotropic. Figure 12 represents the normalized spectrum function for $R_\lambda \approx 1500$, together with the wave numbers representing the frequency of the antialiasing filter, the probe size, and the time response of the probe. It appears that, in this case, the low level of noise, the filtering, the spatial resolution, and the time response of the probe allow us to determine integral (4) reasonably well. For some other files—typically at large Reynolds numbers or low pressures—the presence of noise at large frequencies makes it difficult to use the spectral method; in such cases, we discard the measurement of the skewness made by any of the two methods (spectral and direct).

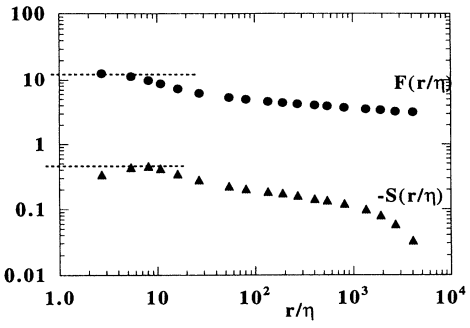

FIG. 11. Evolution of the skewness $-S(r)$ and flatness $F(r)$ of the velocity increments, with the reduced scale r/η, for $R_\lambda \approx 1548$; in this case, $\eta \approx 8.4$ μm and $l_w/\eta \approx 1$. The broken lines correspond to the values of $-S$ and F which we have used in Fig. 13.

We now are in a position to investigate the evolution of the skewness and flatness of the velocity derivatives with respect to the microscale Reynolds number. The corresponding values, obtained by direct or spectral methods (both give same results, within 20%), are displayed in Fig. 13 for cells 1 and 2, using sensors 1, 2, A, B, F, and A'. Interesting information can be extracted from the curve of Fig. 13, which is the main issue of the paper.

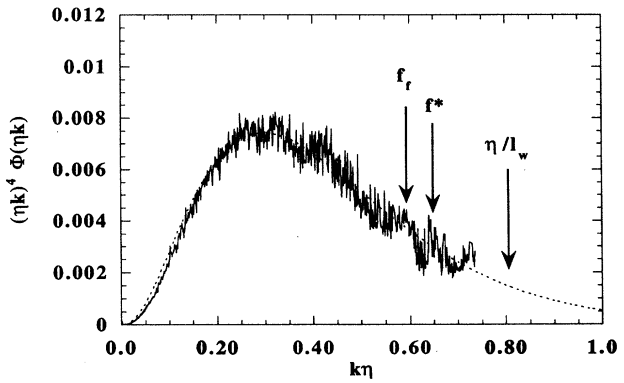

FIG. 12. Plot of the integrand of expression (3), for $R_\lambda \approx 1340$. In this case, the Kolmogoroff scale is 5.6 μm, the mean velocity is 75 cm/s, the sampling frequency is 31 kHz, and the low pass filter frequency is 12 kHz. The dashed line is the expression $1.13\,(k\eta)^{2.28}\exp[-7.6(k\eta)]$.

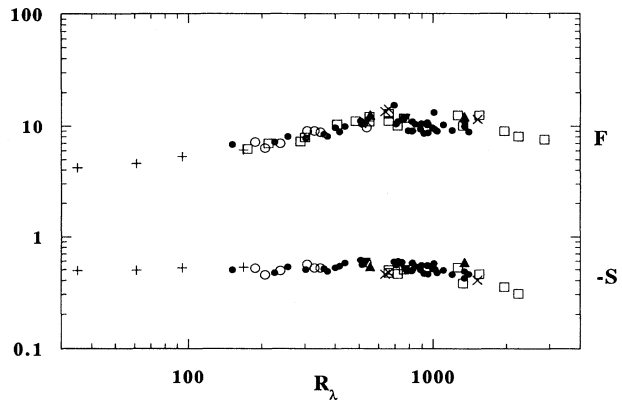

FIG. 13. Evolution of the skewness and flatness factors, S and F, with R_λ. The various symbols are ○, cell 1 , probe 1; □, cell 2, probe B; ●, cell 2, probe A'; +, numerical results [6]; ▼, cell 1, probe 2; ×, cell 2, probe F; ▲, cell 2, probe A.

The few measurements performed with sensor 1 and probes A and F indicate that the skewness and flatness factors are independent of the length and location of the probe. Also, there is no visible difference between the large and small cells, and different fluctuation rates. Moreover, it is interesting to see that, for the lower range of values of the Reynolds number (up to $R_\lambda \approx 700$), there is reasonable agreement between our values and the numerical study of Ref. [6], and more generally with the current experimental findings, as collected in Ref. [4]. We thus find that $-S$ and F increase with the Reynolds number in this range, up to $R_\lambda \approx 700$. But the striking observation which we make, both on $-S$ and F, is that, beyond this range, these two quantities cease to increase. They even show a tendency to decrease with R_λ, although owing to the scatter, it is difficult to conclude. The curve of Fig. 13 suggests two regimes, separated by a transition located around $R_\lambda \approx 700$ (which is a crude estimate). We therefore obtain the somewhat surprising result that, above the transition, the system becomes less and less intermittent in the dissipative range as the Reynolds number increases. This is not contradictory with the statement that the PDF of the velocity increments are independent of R_λ in the inertial range. Both statements simply imply that the size of the domain lying between the inertial and dissipative ranges—measured in units of the Kolmogorov scale—increases (which we do observe).

VI. FURTHER COMMENTS ON THE MEASUREMENTS

The determination of the skewness and flatness of the velocity derivatives is a delicate measurement, since the fluctuations which contribute most to these quantities are rare and belong the high frequency range. It is thus worth discussing, before commenting on the significance of results, some possible sources of error. There are many; we have selected here three of them, which, at the present time, may require some discussion.

Concerning the delicate point of the spatial resolution, the ratio l_w/η is smaller than 3 for all the values of R_λ which we have investigated. It would be indeed desirable to achieve better resolution, but, according to previous work [14], it seems that the ratio of 3 is low enough to determine S within 10%. The corresponding uncertainty of F has been examined recently, in a numerical study [15], and it is found to be equal to 2% for the same conditions. Note that the last estimate must be taken with care because it has been estimated at small R_λ; it turns out that, by comparing sensors of different lengths, we find values consistent with [14] and [15], even at large R_λ. We therefore may consider that the limited probe resolution only introduces a small error into the determination of S and F.

Uncertainties generated by the levels of the fluctuation rates is also an important issue. Previous investigations have led to somewhat different conclusions: according to Ref. [16], we expect, with a fluctuation level of 35%, to overestimate the skewness of the velocity derivatives by 40%, while Ref. [17] gives 4% for the same quantity (the calculation is carried out by assuming that our flow has the structure of a mixing layer [10]). We have compared, for the same R_λ, records with different fluctuation rates; the variations of S which we observe, when the fluctuation rate is varied from 14% to 40%, are hardly distinguishable from the noise. The same result holds for the flatness. We therefore tend to conclude that, in consistency with Heskestad's calculation [17], the error generated by the application of the Taylor hypothesis is small compared to other sources. We have not introduced any correction scheme for the values of S and F, due to the application of the Taylor hypothesis.

The uncertainty related to the fact that the Reynolds number, calculated on the probe diameter, is somewhat large at the extreme values of R_λ, is more difficult to estimate (as mentioned in Sec. III, this number varies from 0.4 to 300 as R_λ is varied from 150 to 2700). However, it is possible to have a rough estimate of the effect of such a large Reynolds number by comparing cells 1 and 2; it turns out that there is no appreciable difference, at least up to $R_\lambda = 1200$. Moreover, one must note that the onset of vortex shedding seems well beyond the transition Reynolds number. Therefore, for this particular source of error, one may also consider that the probe is operated in an acceptable condition.

VII. DISCUSSION AND CONCLUSION

The striking observation which we make is the existence of a transition behavior in the dissipative range. Transitions in high Reynolds number flows have been observed in Rayleigh-Bernard experiments [18], but never in ordinary turbulence [19].

Beyond the problem of the physical significance of our results, an intriguing fact which must be outlined is that they are in conflict with the compilation of Ref. 4, for $R_\lambda > 700$. All that we can say at the present stage is that we do not understand the origin of such a discrepancy. Does this imply that the skewness and flatness are not universal quantities? In particular, is it possible that the

threshold value of R_λ which we find for the transition depends on the flow configuration? Must we have strong doubt about the skewness and flatness measurements at large R_λ (including ours)? All these are indeed acceptable questions. On our side, we shall try to develop additional checks, and to investigate other flow configurations. Concerning the experiments performed in air, we may hope that additional high quality data will become available soon, coming from large wind tunnel experiments and recent studies on atmospheric turbulence; then we might be in better position to resolve some of these issues.

If we accept the existence of a transitional behavior (which is one possible interpretation of Fig. 13—but not the only one [20]), many questions arise. It seems that this transitional behavior is global, since it is observed in several places in the system. It is not related to the turbulence around the blades; otherwise, it would not be observed on probe F. It is not associated with a change in the large scale flow, since nothing is observed on large scale quantities, such as the fluctuation rate and the integral scale; also, its signature on the inertial quantities is not easy to detect. Thus this transitional behavior seems to take place primarily in the dissipative range. We have no element which allows us to propose an origin for such a transitional behavior, but it is tempting to speculate on the following dynamical scenario, which somehow follows a numerical study by Jimenez *et al.* [6]. One may consider that, particularly at large Reynolds numbers, the flatness of the velocity derivatives is controlled by intense vortex filaments, denamed as "worms." Since their characteristic velocity (i.e., the velocity increment across them) is the standard deviation of the large scale velocity, and their diameter is a few Kolmogorov scales, it follows that their Reynolds number increase with R_λ; as already quoted in Ref. [6], this raises the issue of their stability at large Reynolds numbers. We speculate that the transition which we observe corresponds to the instability of such worms [21]. Becoming unstable, they tend to fill more space, and then the flatness (and, to a lesser extent, the skewness) of the velocity derivatives cease to increase with the Reynolds number.

ACKNOWLEDGMENTS

The authors acknowledge A. Arneodo, M. E. Brachet, O. Cadot, B. Castaing, Y. Couder, S. Douady, U. Frisch, Y. Gagne, J. Jimenez, L. Kadanoff, A. Libchaber, D. Lohse, V. L'vov, I. Procaccia, and J. Wang for interesting discussions related to this experiment. They are indebted to K. R. Sreenivasan for crucial remarks on the probe response. They also acknowledge V. Emsellem for computing the thermal field around the probe. This work has been supported by CNRS, Universities Paris VI and Paris VII, Ecole Normale Superieure, and a grant from DRET No. 92/114.

[1] See A. S. Monin and A. M. Yaglom, *Statistical Fluid Mechanics* (MIT Press, Boston, 1975), Vol. 2, and references therein; also see a recent review by M. Nelkin, Adv. Phys. **43**, 143 (1994).

[2] Note that early measurements of the skewness have been performed by R. W. Stewart, Proc. Cambridge Philos. Soc. **47**, 146 (1951). Concerning the PDF, a recent reference is B. Castaing, Y. Gagne, and E. Hopfinger, Physica D **46**, 177 (1990).

[3] P. Kalilasnath, K. R. Sreenivasan, and G. Stolovitzky, Phys. Rev. Lett. **68**, 18, 2766 (1992).

[4] C. W. Van Atta and R. A. Antonia, Phys. Fluids **23**, 2 (1980). Note that this compilation did not include the aircraft experiments performed by C. M. Sheih, H. Tennekes, and J. L. Lumley, Phys. Fluids **14**, 201 (1971), which gives, at large Reynolds numbers, substantially lower values for the flatness and skewness factors.

[5] Several modes of intermittency, and their relation to numerics and experiment, have been discussed recently in L. Biferale, Phys. Fluids A **5**, 2 (1993).

[6] J. Jimenez, A. A. Wray, P. G. Saffman, and R. S. Rogallo, J. Fluid Mech. **255**, 65 (1993).

[7] S. Douady, Y. Couder, and M. E. Brachet, Phys. Rev. Lett. **67**, 983 (1991).

[8] O. Cadot, S. Douady, and Y. Couder, Phys. Fluids **7**, 2 (1995).

[9] J. Maurer, P. Tabeling, and G. Zocchi, Europhys. Lett. **26**, 31 (1994).

[10] G. Zocchi, J. Maurer, P. Tabeling, and H. Willaime, Phys. Rev. E **50**, 5 (1994); **50**, 3693 (1994).

[11] We take the same notations as in G. Comte Bellot, Ann. Rev. Fluid Mech. **8**, 209 (1976). Also see J. Hinze, *Turbulence* (McGraw Hill, New York, 1987), Chap. 2; C. Lomas, *Fundamentals of Hot Wire Anemometry* (Cambridge University Press, Cambridge, 1986).

[12] T. von Karman and L. Howarth, Proc. R. Soc. London Ser. A **164**, 192 (1938); A. N. Kolmogorov, C. R. Acad. Sci. USSR **30**, 301 (1941).

[13] This expression can be found in F. H. Champagne, J. Fluid Mech. **86**, 67 (1978).

[14] J. C. Wyngaard, J. Sci. Instrum. **1**, 1105 (1968); **2**, 983 (1969).

[15] J. Jimenez (private communication).

[16] J. L. Lumley, Phys. Fluids **8**, 1056 (1965).

[17] G. Heskestad, J. Appl. Mech. **87**, 735 (1965).

[18] X. Z. Wu, L. Kadanoff, A. Libchaber, and M. Sano, Phys. Rev. Lett. **64**, 18 (1990); **64**, 2140 (1990). See also S. Grossman and D. Lohse, Phys. Lett. A **173**, 58 (1993), who point out that temperature measurements may be affected by probe size effects at such large Rayleigh numbers.

[19] A transition has been recently observed by B. Chabaud, A. Naert, J. Peinke, F. Chilla, B. Castaing, and B. Hebral, Phys. Rev. Lett. **73**, 3227 (1994). The corresponding transition value of R_λ is much lower than ours (it is 180 in their case). It would be interesting to compare the two transitions.

[20] Since the transition is not sharp, it is not so clear that it exists. One could say that the essential information which can be extracted from Fig. 13 is that the flatness factor ceases to increase in some range of Reynolds numbers.

[21] Bursting of vortex filaments has been observed in this system [7]. Actually, as already mentioned in Sec. I, such filaments presumably do not correspond to the worms of Ref. [6] but to objects of larger size.